

# Conventional and Quantitative MRI in a Novel Feline Model of Demyelination and Endogenous Remyelination

Aaron S. Field, MD, PhD,<sup>1\*</sup> Alexey Samsonov, PhD,<sup>1</sup> Andrew L. Alexander, PhD,<sup>2</sup>  
Pouria Mossahebi, MD, PhD,<sup>1</sup> and Ian D. Duncan, BVMS, PhD<sup>3</sup>

**Background:** The feeding of irradiated food to healthy adult cats results in widespread, noninflammatory demyelination of the central nervous system (CNS); a return to a normal diet results in endogenous remyelination with functional recovery. This recently discovered, reversible disease might provide a compelling clinical neuroimaging model system for the development and testing of myelin-directed MRI methods as well as future remyelination therapies.

**Purpose:** Identify the noninvasive imaging characteristics of this new disease model and determine whether it features measurable changes on conventional and quantitative MRI.

**Study Type:** Pilot study.

**Animal Model:** Ten adult cats at various stages of demyelinating disease induced by an irradiated diet (35–55 kGy), and during recovery following a return to a normal diet.

**Field Strength/Sequence:** Conventional ( $T_2$ -weighted) and quantitative (diffusion tensor, magnetization transfer) at 3T.

**Assessment:** MRI of the brain, optic nerves, and cervical spinal cord; a subset of diseased cats was euthanized for comparative histopathology.

**Statistical Tests:** Descriptive statistics.

**Results:** Disease produced  $T_2$  prolongation, progressing from patchy to diffuse throughout most of the cerebral white matter (eventually involving U-fibers) and spinal cord (primarily dorsal columns, reminiscent of subacute combined degeneration but without evidence of B12 deficiency). Magnetization transfer parameters decreased by 50–53% in cerebral white matter and by 25–30% in optic nerves and spinal cord dorsal columns. Fractional diffusion anisotropy decreased by up to 20% in pyramidal tracts, primarily driven by increased radial diffusivity consistent with axon preservation. Histopathology showed scattered myelin vacuolation of major white matter tracts as well as many thin myelin sheaths consistent with remyelination in the recovery phase, which was detectable on magnetization transfer imaging.

**Data Conclusion:** Feline irradiated diet-induced demyelination features noninvasively imageable and quantifiable demyelination and remyelination of the CNS. It is therefore a compelling clinical neuroimaging model system.

**Level of Evidence:** 4

**Technical Efficacy:** Stage 2

J. MAGN. RESON. IMAGING 2019;49:1304–1311.

Myelin plays a vital role in maintaining axon functional integrity and its loss results in severe clinical dysfunction. Remyelination restores nerve conduction and is proposed to induce neuroprotection<sup>1</sup>; thus, a complete understanding of remyelination is critical in devising therapeutic strategies that

will promote the repair of myelin lesions in multiple sclerosis (MS) and other myelin disorders. To gain such understanding and help guide the development of novel therapeutics that promote myelin repair and neuroprotection, noninvasive testing is required to observe demyelination and remyelination in life.

View this article online at [wileyonlinelibrary.com](http://wileyonlinelibrary.com). DOI: 10.1002/jmri.26300

Received May 24, 2018, Accepted for publication Jul 31, 2018.

\*Address reprint requests to: A.S.F., Department of Radiology, University of Wisconsin, 600 Highland Ave., M/C 3252, Madison, WI 53792.  
E-mail: [afield@uwhealth.org](mailto:afield@uwhealth.org)

From the <sup>1</sup>Department of Radiology, University of Wisconsin School of Medicine and Public Health, Madison, Wisconsin, USA; <sup>2</sup>Department of Medical Physics, University of Wisconsin School of Medicine and Public Health, Madison, Wisconsin, USA; and <sup>3</sup>Department of Medical Sciences, University of Wisconsin School of Veterinary Medicine, Madison, Wisconsin, USA

This is an open access article under the terms of the Creative Commons Attribution-NonCommercial License, which permits use, distribution and reproduction in any medium, provided the original work is properly cited and is not used for commercial purposes.

Many studies in animal models of MS and other myelin diseases have yielded noninvasive imaging markers correlated with myelin and/or axonal status but it has been problematic to identify a metric that is specific for one or the other because in many model systems the axonal and myelin content are themselves highly correlated, resulting in many “secondary” correlations<sup>2–4</sup>; moreover, the pathological changes that exist (eg, inflammation, de-/re-myelination, axon loss, gliosis) often outnumber the imaging metrics aimed at them, even in multivariate approaches, resulting in a statistically intractable analysis problem. This paradox points to the need for a more reductionist model<sup>5</sup> of relatively “pure” de-/re-myelination to effectively calibrate imaging metrics before applying them in more complex systems. One popular example is cuprizone intoxication in the mouse, which is characterized by reversible demyelination<sup>6–11</sup>; however, this model is limited, as it produces no clear clinical phenotype and it affects restricted areas of the central nervous system (CNS), such that it cannot be used to study remyelination in critical areas notably affected in MS, such as the optic nerve or spinal cord, where there are potentially important regional differences in axon size. Thus, alternative experimental models are needed in which there is more widespread demyelination and endogenous remyelination.

A highly novel and unique example of such a model was recently reported,<sup>12</sup> named FIDID (feline irradiated diet-induced demyelination). Briefly, cats fed an irradiated diet (>30 kGy) develop a late-onset, progressive neurologic disease resulting from severe demyelination of the spinal cord, optic nerves, and to a lesser extent, brain. Return to a normal diet early in the disease leads to functional recovery through extensive CNS remyelination.<sup>12</sup> The purpose of this pilot study was to determine whether the FIDID model would produce measurable changes on magnetic resonance imaging (MRI) using a human scanner and clinically translatable image acquisition protocols. We sought to characterize both conventional ( $T_2$ -weighted) and quantitative (magnetization transfer, diffusion tensor) MRI changes associated with this disease and recovery in order to develop a clinical neuroimaging model system for testing myelin-directed MRI methods and, ultimately, novel remyelination therapies.

## Materials and Methods

### Experimental Animals

FIDID was induced in 10 cats by feeding them an irradiated diet (35–55 kGy, cobalt source, Steris Isomedix, Libertyville, IL). Cats developed neurologic disease after 5½ to 6 months of eating this diet and were monitored daily for progression of neurologic dysfunction (ataxia, paresis) which was rated as mild ataxia (+), moderate ataxia and paresis (++), severe ataxia and paresis (+++), or severe with urinary incontinence (++++). Further details regarding the clinical course of the disease are provided in an article submitted elsewhere and currently under review (Radcliff et al, unpublished data). Some

cats, after they reached the moderate/severe disease stage (++ or +++/++) (~6–7 months), were returned to a normal diet and allowed to recover under daily clinical observation. FIDID cats were selected from mild, severe, and partially recovered disease stages for MRI of the brain, optic nerves, and spinal cord followed by perfusion for histopathological analysis, as detailed below. Onset of disease was consistently around 6 months after starting the diet; recovery time on return to a normal diet varied but was at least 4 weeks. The times of sampling of cats for scanning and euthanasia were chosen to represent a spectrum of the MRI changes associated with different stages of the disease.

### MRI

Cats were anesthetized using isoflurane and imaged on a 3.0T GE Discovery MR750 clinical scanner (GE Healthcare, Waukesha, WI) using an eight-channel, phased-array, transmit/receive knee coil which was well-sized for the feline head. Cats were positioned in the coil such that the optic nerves and upper cervical spinal cord were included in the field of view (FOV) along with the brain. Imaging sequences included conventional  $T_2$ -weighted fast spin echo (repetition time [TR] = 11 sec, echo time [TE] = 120 msec, echo train length = 23, matrix =  $320 \times 320 \times 48$ , FOV =  $12 \times 12 \text{ cm}^2$ , slice thickness = 1.5 mm, fat saturation, 4 averages) along with magnetization transfer imaging (MTI) and diffusion tensor imaging (DTI). MTI was performed using two protocols based on 3D spoiled gradient echo (SPGR) acquisitions, one for calculation of standard MT ratio (MTR)<sup>13</sup> and the other for calculation of MT saturation (MTSat),<sup>14</sup> which is believed to be more myelin-specific than MTR and less susceptible to inhomogeneities of the receiver coil and the transmitted RF field.<sup>15</sup> A substantially higher spatial resolution is required for spinal cord and optic nerve imaging relative to the much larger brain; therefore, in order to stay within acceptable scan time limits, MTR was used in the cord and optic nerves (as it uses fewer scans) and MTSat in the brain. For MTR calculation, two  $T_2$ -weighted 3D SPGR scans were acquired with TR/TE = 35/4.6 msec, flip angle =  $17^\circ$ , one with an MT pre-pulse (8 msec Fermi pulse, 2.5 kHz offset frequency, effective flip angle of  $670^\circ$ ), and one with a different offset frequency (200 kHz) to have no MT effect. The acquisition matrix was  $320 \times 320 \times 128$  with FOV =  $10 \times 10 \text{ cm}^2$ , ST = 0.8 mm, 4 averages. The MTSat protocol consisted of proton density (PD)-weighted,  $T_1$ -weighted, and MT-weighted data, all acquired with matrix =  $192 \times 192 \times 56$ , FOV =  $12 \times 12 \text{ cm}^2$ , ST = 1.2 mm. PD- and  $T_1$ -weighted images were acquired with two 3D SPGR scans at TR/TE = 18/3.3 msec with flip angles  $4^\circ$  and  $30^\circ$ , respectively. MT-weighted images were acquired with TR/TE = 28/3.3 msec, flip angle  $10^\circ$ , 8 ms Fermi MT pulse at  $790^\circ$  effective flip angle and 3 kHz offset frequency. DTI data were acquired using a conventional single-shot spin echo, echo-planar imaging sequence as follows: TR/TE = 5000/87 msec, matrix =  $128 \times 128 \times 33$ , ST = 2 mm, FOV =  $12 \times 12 \text{ cm}^2$ ,  $b = 1000 \text{ s/mm}^2$ , 55 diffusion directions, 2× ASSET acceleration, and 2 averages. Acquisition times exceeded what would be feasible in clinical practice because of the demands for higher spatial resolution in the much smaller structures of the feline brain and spinal cord. However, with lesser demands for spatial resolution in the human brain, each of the imaging sequences used in this study could be completed in under 10 minutes as part of a clinical scan protocol.

### MTI Processing

Standard MTR was calculated in spinal cord and optic nerves along with MTSat in the brain, MTSat being more independent of system parameters and  $T_1$  weighting, and therefore believed to be more myelin-specific than MTR, at the expense of greater scan time. All source datasets were first coregistered using the Functional MRI of the Brain (FMRIB) Software Library (FSL) Image Registration tool (FLIRT) (Oxford, UK). MTR was then calculated as a difference between images acquired without and with MT saturation and normalized by the former. Calculation of MTSat followed the original method described by Helms et al.<sup>14</sup> White matter was segmented using the FSL Automated Segmentation Tool (FAST) in order to derive mean MTSat for whole-brain white matter, which might be sensitive to nonfocal changes not readily apparent by visual inspection.

### DTI Processing

DTI images were corrected for eddy-current distortion prior to coregistration and then postprocessed using FSL software to generate maps of fractional anisotropy (FA), mean diffusivity (MD), axial diffusivity (AD), and radial diffusivity (RD), where AD is the major eigenvalue, RD is the average of the medium and minor eigenvalues, MD is the average of all three eigenvalues, and FA is the normalized variance of all three eigenvalues of the diffusion tensor. Given the technical limitations of DTI, image quality was satisfactory in the brain only. DTI images were subjected to manual region-of-interest (ROI) analysis rather than white matter segmentation because, unlike MTSat, whole-brain white matter DTI measures may be contaminated by well-known partial volume effects at the boundaries between perpendicularly crossing fiber tracts.

### Histological Analysis

At termination, cats were euthanized, then immediately perfused through the aorta with 4% paraformaldehyde (PFA) or a modified Karnovsky fixative. The brain and spinal cord were removed and following at least 1 week postfixation, were trimmed for processing for either embedding in paraffin or in epon (spinal cord) for sectioning and staining. Paraffin sections of the brain were stained with hematoxylin and eosin (H&E) or Luxol fast blue. One-micron sections from the spinal cord were stained with toluidine blue (all neuropathological details assessed by I.D.D., who has 30 years' experience as a neuroscientist).

All of the materials and methods detailed above were part of an Institutional Animal Care and Use Committee (IACUC)-approved protocol.

## Results

### Conventional ( $T_2$ -Weighted) MRI

Conventional images were subjectively assessed by A.S.F., who has 20 years experience as a clinical neuroradiologist. Severely affected cats developed a largely diffuse, ill-defined pattern of  $T_2$  prolongation (hyperintensity) throughout most of the cerebral white matter involving both the deep white matter and subcortical arcuate tracts, resulting in diminished or reversed gray–white matter contrast (Fig. 1). Partial sparing of corpus callosum and internal capsules was noted in all

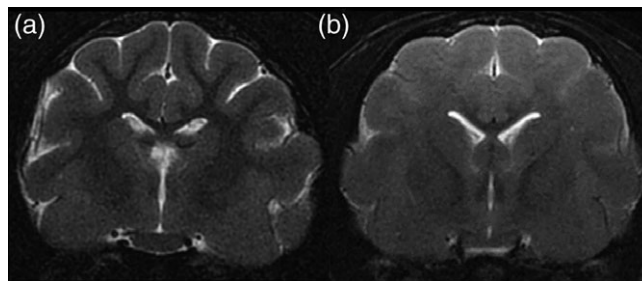


**FIGURE 1:** Conventional  $T_2$ -weighted images acquired in vivo in a normal cat (a) and a severely affected cat (clinical score +++) after 28 weeks on an irradiated diet (b). Cerebral white matter is diffusely hyperintense in the affected cat, resulting in diminished gray–white contrast (b). Portions of corpus callosum and internal capsules are spared, retaining their normal hypointensity relative to gray matter. Generalized brain swelling is evidenced by diminished visibility of cortical sulci.

animals (Fig. 1b). There was generalized brain swelling evidenced by diminished visualization of cortical sulci (Fig. 1b). At milder stages of disease, the white matter involvement was patchier, with relative sparing of subcortical arcuate fibers and less brain swelling (Fig. 2). These changes were partially reversible following a return to a normal diet (Fig. 3) except in the case of more advanced disease.

In the spinal cord, severely affected cats developed  $T_2$  prolongation primarily involving the dorsal columns, a pattern reminiscent of subacute combined degeneration (SCD) in humans.<sup>16</sup> In the optic nerves, no significant  $T_2$ -weighted signal changes were observed, although spatial imaging resolution was likely insufficient in these very small structures; MTI acquired at higher resolution did reveal changes in the optic nerves, as detailed below.

### MTI

Severely affected cats developed a widespread decrease in MTSat throughout most of the cerebral white matter with portions of corpus callosum and internal capsules spared, similar to the observed pattern of  $T_2$  prolongation but generally much more readily visible compared to the  $T_2$ -weighted images (Fig. 4). These changes were partially reversible following a return to a normal diet but this reversal lagged

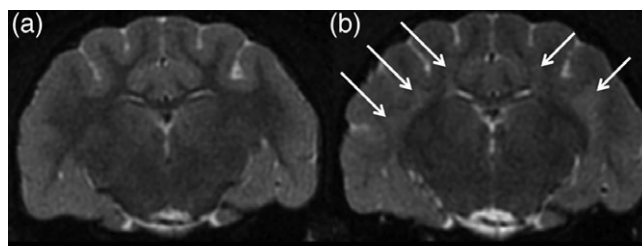


**FIGURE 2:** Conventional  $T_2$ -weighted images acquired in vivo in a cat at normal baseline (a) and the same animal after 22 weeks on an irradiated diet (clinical score +++/++++) (b). The white matter  $T_2$  prolongation in this animal is more patchy (arrows) than in other cats at advanced disease stages (cf. Fig. 1), with relative sparing of subcortical arcuate fibers.

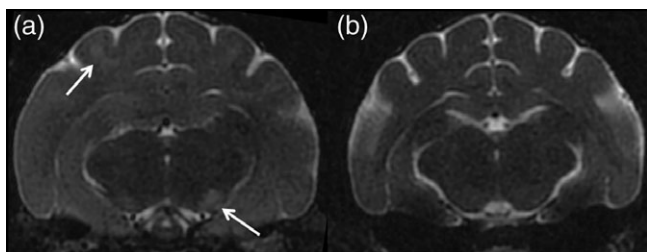


**FIGURE 3:** Conventional T<sub>2</sub>-weighted images acquired *in vivo* in one severely affected cat (clinical score +++) after 29 weeks on an irradiated diet (a) and the same animal 18 weeks after a return to a normal diet (clinical score +/-) (b). Diffuse hyperintensity in the subcortical white matter and a more focal hyperintense lesion in the left crus cerebri (arrows) are seen to be reversible.

functional recovery. (Remyelinated axons approach normal conduction velocities with as few as five myelin lamellae,<sup>17</sup> which may be insufficiently thick for detection by MRI; hence, functional recovery may precede final, MRI-detectable ensheathment.)

FAST-segmented whole-brain white matter mean MTSat (Fig. 5) decreased by 50–53% from normal to severe disease. In spinal cord and optic nerves, given the small size of these structures, only MTR was acquired, as higher signal-to-noise ratio (SNR) and spatial resolution can be attained within the same imaging time compared to MTSat. MTR decreases of 25–30% were measured in the optic nerves and in the dorsal columns of the spinal cord (Fig. 6a,b), with lesser reductions (5–10%) in the lateral and ventral columns.

### DTI

In contrast to the T<sub>2</sub>-weighted images and MTI in the brain, no significant disease-related changes were immediately apparent on visual inspection of FA maps (Fig. 7). We speculate that this is because axons, which are the primary determinant of diffusion anisotropy in neural tissue,<sup>18</sup> are largely preserved in this

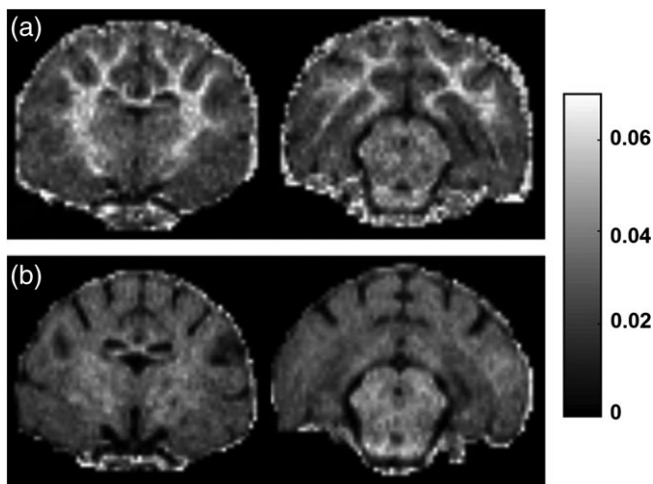


**FIGURE 4:** MTSat maps for two axial sections of a normal cat (a) and a severely affected cat (clinical score +++) after 29 weeks on an irradiated diet (b). Decreased MTSat is widespread throughout the cerebral white matter except for a few spared portions of corpus callosum and internal capsules.

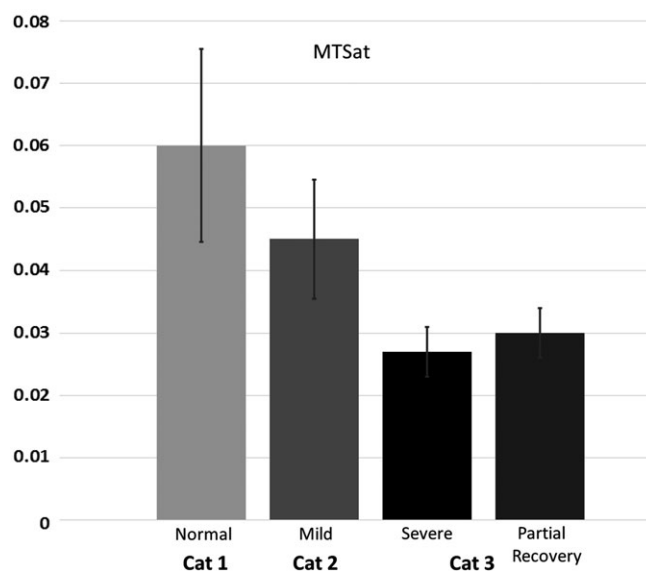


**FIGURE 5:** Whole-brain white matter MTSat (mean ± SE) in three cats: Cat 1 is normal and Cat 2 is mildly affected (35 weeks on an irradiated diet, clinical score ++); Cat 3 is shown at severe disease stage (29 weeks on an irradiated diet, clinical score +++) and during partial functional recovery (18 weeks after return to normal diet, clinical score +/-).

disease model. However, there were measurable decreases in FA. From normal to severe disease, FA in the internal capsules (the most reproducibly measured tract) decreased from 0.68 to 0.53 (22%). This decrease reflected both an increase in radial diffusivity (from  $0.387 \times 10^{-3}$  to  $0.481 \times 10^{-3}$  mm<sup>2</sup>/s or 24%) and a concomitant but relative smaller decrease in axial diffusivity (from  $1.42 \times 10^{-3}$  to  $1.19 \times 10^{-3}$  mm<sup>2</sup>/s or 16%).

### Histopathology

Coronal sections of the brain showed scattered myelin vacuolation of the major white matter tracts of variable severity (Fig. 8). The optic tracts and adjacent cerebral peduncles were the most vacuolated structures. The corpus callosum was also vacuolated but was variable, as the medial aspect of the callosum showed moderate vacuolation while the lateral aspects appeared normal. Notable but scattered vacuolation of the internal capsules and subcortical white matter was seen.

The C1-level segment of the cervical spinal cord, which directly corresponded to the MTSat map shown in Fig. 6b, was severely affected—especially the dorsal columns, which showed demyelination and remyelination of the subpial area, but marked axon loss in the core of the dorsal column or fasciculus gracilis (Fig. 6c). The adjacent white matter to the fasciculus gracilis, ie, fasciculus cuneatus, had many preserved myelinated axons, some of which had thin myelin sheaths (ie, remyelinated); likewise, the base of the dorsal column appeared to be normally myelinated, with only occasional thin myelin sheaths. Despite this severe lesion of the dorsal column, the clinical score of this cat was +/-+. Loss of axons in the fasciculus gracilis appears, therefore, not to produce marked ataxia or paresis.

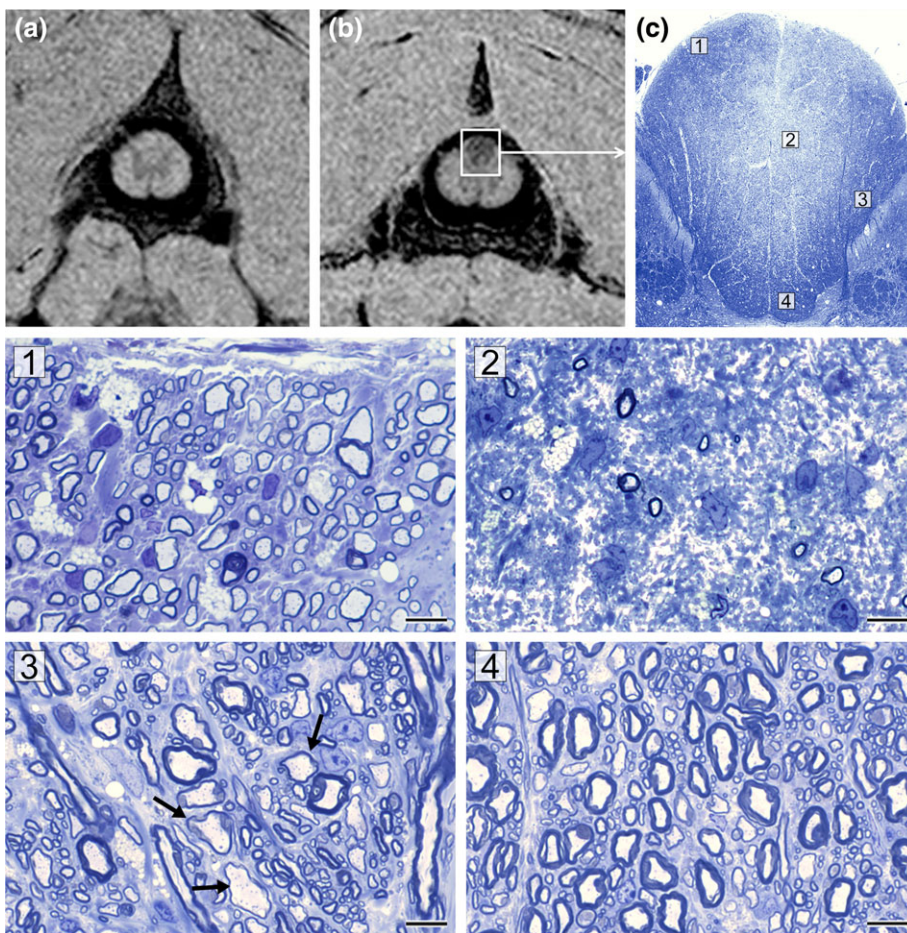


**FIGURE 6:** MTR maps in C1-level cervical spinal cord of normal cat (a) and affected cat after 29 weeks on an irradiated diet (clinical score + /++) (b) show decreased MTR most readily apparent in the dorsal columns (magnification box). The corresponding tissue section of the whole dorsal column (c) shows that its core, which contains fibers predominately from the fasciculus gracilis, is pale compared to the surrounding dorsal, lateral, and ventral parts. Four labeled areas (1–4) are shown in higher power on the bottom. The subpial zone of the fasciculus gracilis (1) contains only thinly remyelinated axons, whereas the core of the FG has very few surviving axons (2). The fasciculus cuneatus contains both remyelinated and normally myelinated axons (3), whereas the deep white matter appears normally myelinated (4).

**Discussion**

Presented herein are the conventional and quantitative MRI findings in FIDID, a highly novel animal model of non-inflammatory demyelination and remyelination with functional

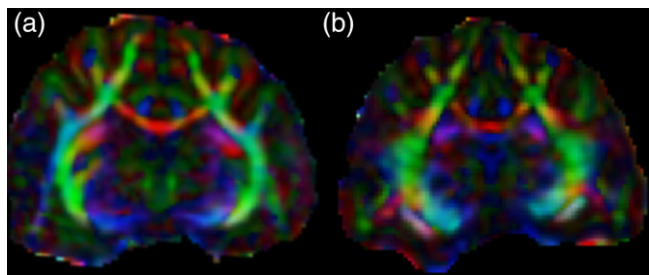


**FIGURE 7:** FA maps with directional color encoding (red: left-right; green: dorsal-ventral; blue: rostral-caudal) in a normal cat (a) and a severely affected cat (clinical score +++) after 27 weeks on an irradiated diet (b). Diffusion anisotropy is largely preserved in the affected cat, presumably reflecting the preservation of axons, which are the primary determinant of anisotropic diffusion in neural tissue.<sup>16</sup>

recovery resulting from the feeding of irradiated food (>30 kGy) to healthy adult cats.<sup>12</sup> Our specific aim was to determine whether this model would produce measurable MRI changes (and if so, to characterize them) using a human scanner and clinically translatable image acquisition protocols. The overarching goal was to develop a reductionist, clinical neuroimaging model system for testing myelin-directed MRI methods and, ultimately, novel remyelination therapies.

To the extent that it resembles any human disease, the FIDID model bears the most similarity to SCD. Originally described in association with pernicious anemia, but now known to occur with other vitamin B12 deficiency states,<sup>19</sup> SCD is characterized by noninflammatory vacuolation and subsequent degeneration of myelin, primarily in the dorsal columns of the spinal cord, resulting in a clinical syndrome that may include lower extremity paresthesia, ataxia, spastic paraplegia, and incontinence.<sup>19</sup> The FIDID model shares both the clinical and conventional MRI findings of SCD—namely, T<sub>2</sub>-hyperintensity primarily involving dorsal columns—but there

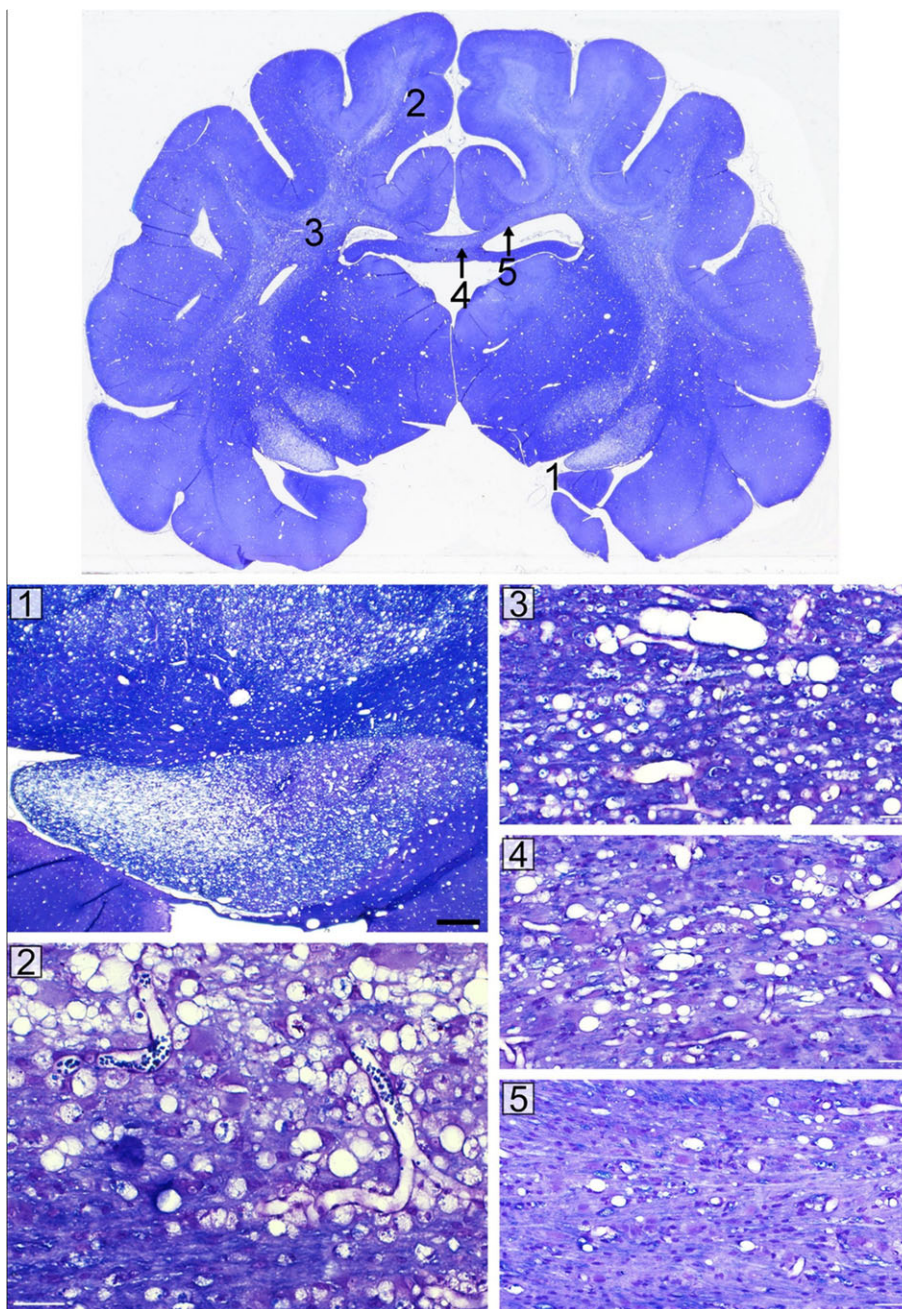


**FIGURE 8:** This coronal midbrain section shows scattered and variable myelin vacuolation from a cat with clinical score +++. The most severely affected areas include the optic tracts and cerebral peduncles (1). The internal capsules (3) and subcortical white matter (2) show scattered, marked vacuolation. The corpus callosum is vacuolated in the midline (4) but not in its lateral aspects (5). Corresponding enlargements of each of these areas are shown in the bottom panels (1–5).

is no biochemical evidence of a B12 deficiency (blood levels of cobalamin, folate, methylmalonic acid, and homocysteine all normal) (Radcliff et al, unpublished data). As examples of relatively “pure” demyelination, both SCD and FIDID offer some advantages as reductionist models for purposes of noninvasive imaging study; however, quantitative imaging in these conditions to date is limited in SCD and lacking in FIDID. Conventional MRI findings in SCD are well known in spinal cord but only sporadically reported in the brain.<sup>20,21</sup> DTI has revealed brain microstructural changes in SCD that were occult to conventional MRI.<sup>22</sup> As for remyelination, the spinal cord

abnormalities observed in SCD can be either reversible with B12 therapy or irreversible.<sup>23</sup> We have found similar variations in FIDID, but the nature and significance of this variability and the point at which the disease becomes irreversible, presumably through axon loss, are poorly understood yet highly relevant (not only to SCD but other demyelinating conditions including MS that may be amenable to remyelination before the conversion to irreversibility occurs).

Although conventional T<sub>2</sub>-weighted imaging is notoriously lacking in both sensitivity and specificity, it remains a clinically relevant modality in white matter disease and it did

qualitatively reveal the profound, widespread demyelination and vacuolation occurring on the irradiated diet. Regional variations in  $T_2$ -weighted signal intensity (eg, relative sparing of corpus callosum and internal capsule) were confirmed by the histology.

Magnetization transfer (MT) imaging exploits the transfer of proton spin magnetization between “free” and “bound” pools of protons to estimate the quantity of macromolecules in tissue; given the preponderance of macromolecules in membrane proteins and long-chain fatty acids of the myelin sheath, MT metrics including MT ratio (MTR) and MT saturation (MTSat) are widely regarded as “myelin markers,” although their specificity is actually rather limited.<sup>3,24</sup> In a reductionist model such as FIDID, where the tissue changes (at least early in disease course) appear limited to demyelination and are reversible through endogenous remyelination, concerns over specificity are likely mitigated such that MT metrics do essentially function as myelin markers. We observed MTSat reductions on the order of 30% and 50% in the cerebral white matter of cats with mild and severe disease, respectively, and a slight increase reflecting (incomplete) remyelination in a partially recovered cat. In more complex systems, greater sensitivity and specificity are required, potentially achievable through more sophisticated modeling of the MT effect (so-called “quantitative MT” or qMT).<sup>25–27</sup> For example, in a previous study of the dysmyelinating mutant *shaking* (*sh*) pup, the macromolecular proton fraction (MPF) derived from qMT imaging was the strongest indicator distinguishing mutant from wildtype animals and detected the increase in myelination with aging in the *sh* pup, whereas MTR did not.<sup>15</sup> More recently, MPF closely agreed with histological myelin staining in the cuprizone mouse model.<sup>28</sup> QMT imaging was technically prohibitive in the feline model, but those problems have since been solved and qMT will be employed in future work with this model.

DTI exploits the anisotropic diffusion of water molecules in nerve fiber bundles to measure their microstructural integrity. Although anisotropy metrics (most commonly FA) tend to be higher in myelinated than unmyelinated or demyelinated nerve fibers, reflecting the hindrance of diffusion by the multilayered myelin sheath, the primary determinant of anisotropy in fact is not myelin but axonal membranes.<sup>18</sup> Therefore, FA conceivably could serve as either a myelin or axonal marker in applications where only one or the other was expected to change. Such is often not the case, however, and this complexity has motivated a more sophisticated approach to diffusion modeling in tissue. For example, there is evidence that increased radial and decreased axial diffusion (at least to a first approximation) reflect separately demyelination and axonal degeneration, respectively.<sup>29</sup> We observed anisotropy reductions primarily driven by increased radial diffusion, as would be expected for demyelination without loss of axons. In future work with this model we will determine

whether and at what stage axial diffusion can detect the eventual loss of axons during a prolonged disease course.

As this was an exploratory pilot study in a small number of cats with significant ethical and cost constraints, we were unable to image and euthanize a sufficient number of animals to enable a rigorously quantitative (ie, statistical) analysis of MR-histopathological correlations. Importantly, however, we have shown for the first time that this highly novel animal model produces quantifiable MRI changes using a human scanner and clinically translatable imaging protocols—a necessary prelude to developing a first-of-its-kind clinical neuroimaging model system for testing myelin-directed MRI methods and, ultimately, novel remyelination therapies. We plan to utilize the FIDID model to study therapeutic strategies that may promote remyelination, including vitamin B12, given the model’s striking resemblance to SCD as well as the vitamin B12 deficiency in nonhuman primates.<sup>30</sup>

In conclusion, FIDID, a highly novel “reductionist” model for the study of myelin disease and repair, features noninvasively imageable and quantifiable demyelination and remyelination of the CNS. Future work will be devoted to validating and calibrating an optimal set of imaging biomarkers capable of tracking myelin loss and repair in order to guide the development of novel therapies for MS and other white matter diseases.

---

## Acknowledgment

Contract grant sponsor: National Multiple Sclerosis Society; Contract grant number: RG-1501-02876.

The authors thank Dr. Abigail Radcliff for assistance with animal care and study coordination.

## References

- Franklin RJM, ffrench-Constant C. Regenerating CNS myelin — from mechanisms to experimental medicines. *Nat Rev Neurosci* 2017;18:753–769.
- Schmierer K, Scaravilli F, Altmann DR, Barker GJ, Miller DH. Magnetization transfer ratio and myelin in postmortem multiple sclerosis brain. *Ann Neurol* 2004;56:407–415.
- Mottershead JP, Schmierer K, Clemence M, et al. High field MRI correlates of myelin content and axonal density in multiple sclerosis—a post-mortem study of the spinal cord. *J Neurol* 2003;250:1293–1301.
- Bot JC, Blezer EL, Kamphorst W, et al. The spinal cord in multiple sclerosis: relationship of high-spatial-resolution quantitative MR imaging findings to histopathologic results. *Radiology* 2004;233:531–540.
- Dubois-Dalq M, ffrench-Constant C, Franklin RJM. Enhancing central nervous system remyelination in multiple sclerosis. *Neuron* 2005;48:9–12.
- Kipp M, Clamer T, Dang J, Copray S, Beyer C. The cuprizone animal model: new insights into an old story. *Acta Neuropathol* 2009;118:723–736.
- Armstrong RC, Le TQ, Flint NC, Vana AC, Zhou YX. Endogenous cell repair of chronic demyelination. *J Neuropathol Exp Neurol* 2006;65:245–256.

8. Arnett HA, Wang Y, Matsushima GK, Suzuki K, Ting JP. Functional genomic analysis of remyelination reveals importance of inflammation in oligodendrocyte regeneration. *J Neurosci* 2003;23:9824–9832.
9. Stidworthy MF, Genoud S, Suter U, Mantei N, Franklin RJM. Quantifying the early stages of remyelination following cuprizone-induced demyelination. *Brain Pathol* 2003;13:329–339.
10. Matsushima GK, Morell P. The neurotoxicant, cuprizone, as a model to study demyelination and remyelination in the central nervous system. *Brain Pathol* 2001;11:107–116.
11. Ludwin SK. Central nervous system demyelination and remyelination in the mouse: an ultrastructural study of cuprizone toxicity. *Lab Invest* 1978;39:597–612.
12. Duncan ID, Brower A, Kondo Y, Curlee JF Jr, Schultz RD. Extensive remyelination of the CNS leads to functional recovery. *Proc Natl Acad Sci U S A* 2009;106:6832–6836.
13. van Buchem MA, McGowan JC, Kolson DL, Polansky M, Grossman RI. Quantitative volumetric magnetization transfer analysis in multiple sclerosis: estimation of macroscopic and microscopic disease burden. *Magn Reson Med* 1996;36:632–636.
14. Helms G, Dathe H, Kallenberg K, Dechent P. High-resolution maps of magnetization transfer with inherent correction for RF inhomogeneity and T1 relaxation obtained from 3D FLASH MRI. *Magn Reson Med* 2008;60:1396–1407.
15. Samsonov A, Alexander AL, Mossahebi P, Wu YC, Duncan ID, Field AS. Quantitative MR imaging of two-pool magnetization transfer model parameters in myelin mutant shaking pup. *Neuroimage* 2012;62:1390–1398.
16. Hemmer B, Glocker FX, Schumacher M, Deuschl G, Lucking CH. Subacute combined degeneration: clinical, electrophysiological, and magnetic resonance imaging findings. *J Neurol Neurosurg Psychiatry* 1998;65:822–827.
17. Felts PA, Baker TA, Smith KJ. Conduction in segmentally demyelinated mammalian central axons. *J Neurosci* 1997;17:7267–7277.
18. Beaulieu C. The basis of anisotropic water diffusion in the nervous system — a technical review. *NMR Biomed* 2002;15:435–455.
19. Russell JSR, Batten FE, Collier J. Subacute combined degeneration of the spinal cord. *Brain* 1900;23:39–110.
20. Crawford JR, Say D. Vitamin B12 deficiency presenting as acute ataxia. *BMJ Case Rep* 2013;2013.
21. Gursoy AE, Kolkukisa M, Babacan-Yildiz G, Celebi A. Subacute combined degeneration of the spinal cord due to different etiologies and improvement of MRI findings. *Case Rep Neurol Med* 2013;2013:159649.
22. Gupta PK, Gupta RK, Garg RK, et al. DTI correlates of cognition in conventional MRI of normal-appearing brain in patients with clinical features of subacute combined degeneration and biochemically proven vitamin B (12) deficiency. *AJNR Am J Neuroradiol* 2014;35:872–877.
23. Pittcock SJ, Payne TA, Harper CM. Reversible myelopathy in a 34-year-old man with vitamin B12 deficiency. *Mayo Clin Proc* 2002;77:291–294.
24. Does MD, Beaulieu C, Allen PS, Snyder RE. Multi-component T1 relaxation and magnetisation transfer in peripheral nerve. *Magn Reson Imaging* 1998;16:1033–1041.
25. Yarnykh VL. Pulsed Z-spectroscopic imaging of cross-relaxation parameters in tissues for human MRI: theory and clinical applications. *Magn Reson Med* 2002;47:929–939.
26. Sled JG, Pike GB. Quantitative imaging of magnetization transfer exchange and relaxation properties in vivo using MRI. *Magn Reson Med* 2001;46:923–931.
27. Mossahebi P, Yarnykh VL, Samsonov A. Analysis and correction of biases in cross-relaxation MRI due to biexponential longitudinal relaxation. *Magn Reson Med* 2014;71:830–838.
28. Khodanovich MY, Sorokina IV, Glazacheva VY, et al. Histological validation of fast macromolecular proton fraction mapping as a quantitative myelin imaging method in the cuprizone demyelination model. *Sci Rep* 2017;7:46686.
29. Song SK, Sun SW, Ju WK, Lin SJ, Cross AH, Neufeld AH. Diffusion tensor imaging detects and differentiates axon and myelin degeneration in mouse optic nerve after retinal ischemia. *Neuroimage* 2003;20:1714–1722.
30. Agamanolis DP, Victor M, Harris JW, Hines JD, Chester EM, Kark JA. An ultrastructural study of subacute combined degeneration of the spinal cord in vitamin B12-deficient rhesus monkeys. *J Neuropathol Exp Neurol* 1978;37:273–299.